Proceedings of IMECE2005
2005 ASME International Mechanical Engineering Congress and Exposition
November 5-11, 2005, Orlando, Florida USA

IMECE2005-79838

ENERGY DISSIPATION WITH SLOSHING FOR ABSORBER DESIGN

Birhan Guzel[1], Mahesh Prakash[2], S. Eren Semercigil[1] and Özden F. Turan[1]

[1]Victoria University
School of Arch. Civil and Mechanical Engineering
Footscray Campus
PO BOX 14428, MCMC
Melbourne, Victoria 8001 AUSTRALIA

[2]CSIRO
Mathematical and Information Sciences
Private Bag 10, Clayton South
VIC 3169 AUSTRALIA

ABSTRACT

Sloshing is the low frequency oscillation of the free surface of a liquid in a partially full container. Due to its detrimental effects, efforts are usually made in the direction of suppressing sloshing. In addition, intentionally induced sloshing may be employed as an effective energy sink to provide protection for resonant structures exposed to excessive vibration levels.

It is generally reported that sloshing absorbers with shallow levels of liquid are more effective energy dissipators than those with deep levels. However, there has not yet been a study to reveal the mechanism of energy dissipation for practical applications, although there has been ample empirical proof for effectiveness. One of the limitations from a numerical perspective lies with the difficulty in predicting extreme free surface behaviour by traditional grid based computational methods. The objective of this paper is to report initial observations in this direction using Smoothed Particle Hydrodynamics (SPH). SPH is a Lagrangian method of solving the equations for fluid flow, that is suitable for modeling free surface phenomena such as sloshing due to its grid-free nature. Results are reported in this paper in the form of numerical case studies.

Keywords: sloshing, shallow, dissipation, energy, SPH

INTRODUCTION

The sloshing behaviour of tuned rectangular tanks have long been an area of study. Utilization of the sloshing in a container is widely popular in the design of Tuned Liquid Dampers (TLDs). A variety of experimental and numerical studies relating to this subject can be found in the literature [1-5], with various suggestions to suppress wind and earthquake induced oscillations for different structures. However, the effectiveness of the energy dissipation characteristics of shallow depth containers has not been studied as widely. A numerical study on the subject has been difficult due to complex free surface behaviour.

SPH has specific advantages in modeling transient, complex flows and free surface behaviour, therefore a computational analysis using the SPH method is considered to be an appropriate tool for this kind of study. The advantages include highly accurate and non-diffusive prediction of wave motion, fragmentation and splashing, accurate and automatic convection of material, and the straightforward inclusion of multiscale multi-physics [6-8]. Among many other applications, SPH has also been utilized in sloshing type problems before [7].

In this paper, change of the dissipation of total kinetic energy in a rectangular tank has been investigated for various liquid depths. Numerical results that are obtained using an SPH method have been analyzed in detail. The findings regarding the relation between shallow liquid depths and effectiveness of energy dissipation is reported.

METHODOLOGY

A computer code that is developed in CSIRO Mathematical and Information Sciences has been used in this study. The code employs the SPH method which is briefly described in the first part of this section. Further information on SPH method can be found in [6]. An explanation of the numerical model used is given in the second part together with the procedure followed in the analysis.

(i) SPH

SPH is a 'particle'-based method for modeling coupled fluid flows, solid-structure deformation and heat transfer. Importantly, SPH does not use any fixed grids or meshes to track the fluid and calculate the fluid velocities. Formally, SPH is a Lagrangian continuum method for solving systems of partial differential equations. The fluid (or solid) is discretized into elements, and the properties of each of the fluid-solid elements are attributed to their centres, which are then interpreted as particles. SPH uses an interpolation kernel to smooth the values of any information held by the particles to give smooth continuous interpolated fields (e.g. smooth density or pressure fields from the discrete values of fluid density and pressure at the particles).

In SPH, each particle 'b' has properties: mass m_b, position r_b, density ρ_b and velocity v_b. The interpolated value of any field A at position r is approximated using information from these particles by,

$$A(r) = \sum_b m_b \frac{A_b}{\rho_b} W(r - r_b, h) \qquad (1)$$

where W is an interpolating kernel, h is the interpolation length, and the value of A at r_b is denoted by A_b. The sum is over all particles 'b' within a radius 2h of r_b.

The SPH continuity equation is,

$$\frac{d\rho_a}{dt} = \sum_b m_b (v_a - v_b) \nabla W_{ab} \qquad (2)$$

The position vector from particle 'b' to particle 'a' is denoted by $r_{ab} = r_a - r_b$ and $W_{ab} = W(r_{ab}, h)$ is the interpolation kernel evaluated for the distance $|r_{ab}|$.

The SPH momentum equation is,

$$\frac{dv_a}{dt} = -\sum_b m_b \left[\left(\frac{P_b}{\rho_b^2} + \frac{P_a}{\rho_a^2} \right) - \frac{\xi}{\rho_a \rho_b} \frac{4\mu_a \mu_b}{(\mu_a + \mu_b)} \frac{v_{ab} r_{ab}}{r_{ab}^2 + \eta^2} \right] \nabla_a W_{ab} + g \qquad (3)$$

where P_a and μ_a are pressure and viscosity of particle 'a' and $v_{ab} = v_a - v_b$. Here, η is a small parameter used to smooth out the singularity at $r_{ab} = 0$, and g is the gravitational acceleration.

The time-step for the explicit integration used in these simulations is limited by the Courant condition modified for the presence of viscosity,

$$\Delta t = \min_a \left\{ \frac{0.5h}{c_s + 2\xi\mu_a / h\rho_a} \right\} \qquad (4)$$

where c_s is the local speed of sound.

SPH is a compressible method for fluid flows, which is used near the incompressible limit by choosing a sound speed that is much larger than the velocity scales in the flow. This quasi-incompressible limit is actually what happens with real fluids. The equation of state, giving the relationship between particle density and fluid pressure is,

$$P = P_0 \left[\left(\frac{\rho}{\rho_0} \right)^{\gamma} - 1 \right] \qquad (5)$$

where P_0 is the magnitude of the pressure ρ_0 is the reference density. For water or liquid metals the exponent $\gamma = 7$ is used [6]. This pressure is then used in the SPH momentum equation to give the particle motion.

The pressure scale factor P_0 is given by,

$$\frac{\gamma P_0}{\rho_0} = 100V^2 = c_s^2 \qquad (6)$$

where V is the characteristic or maximum fluid velocity. This ensures that the density variation is less than 1% and the flow can be regarded as incompressible.

(ii) Numerical Model and Procedure

A (400 mm x 400 mm) rigid container with varying depths of water has been modeled using the SPH software. A sinusoidal displacement function with an amplitude of 50 mm and a frequency of 1.4 Hz is used as the excitation to the base of the container. It should be noted that the peak-to-peak base excitation of 100 mm is $1/4^{th}$ of the length of the container which is chosen to be intentionally large to cause severe displacement at the free surface of the liquid. The model is shown schematically in Figure 1 along with the direction of base excitation.

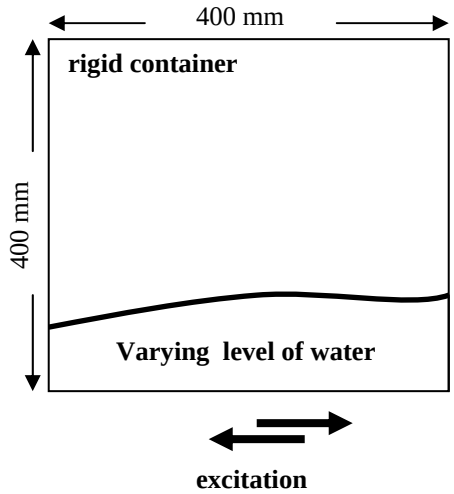

Figure 1. 2-D model used in the numerical simulations.

The numerical simulation conditions were validated in advance to insure that the obtained results are independent of time step and particle size. A single particle in the 2-D model

represents a (0.8 mm x 0.8 mm) area of the water in the container. The time step is implicitly set by assigning a value to V in Equation 6. The SPH simulation progresses by explicitly integrating the system of differential equations (Equations 2 and 3) using the 2nd order Runge Kutta scheme.

Energy dissipation characteristics of five different water depths are predicted numerically for 10 seconds. The rigid container in Figure 1 is filled with 20 mm, 40 mm, 60 mm, 80 mm and 100 mm water. The container is excited with the sinusoidal displacement immediately after a one second period of settling initially. It is also understood that the base displacement imposes increasing amounts of energy to the sloshing liquid, as the mass of water increases with depth. However, what is of more significance here is the rate with which the imposed energy is dissipated relative to the starting value of each case.

RESULTS

Dissipation of kinetic energy due to shearing of the liquid, is the primary means of energy loss in a sloshing liquid. Hence, energy dissipation is enhanced as the velocity gradients in the flow become steeper. For a sloshing liquid, there seems to be two particular events which result in steep velocity gradients, namely wave-to-wall and wave-to-wave interactions. Among the two, wave-to-wave interactions are observed to be more effective dissipators. For a traveling sloshing wave, both type of interactions are available. For a standing sloshing wave, only wave-to-wall interaction is available. Hence, a traveling wave seems to have the advantage. The following discussion in this paper, is to provide details of this argument making reference to specific cases.

History of the total kinetic energy is presented in Figure 2 for all the cases simulated as part of this study. Figures 2(a) to 2(e), correspond to the liquid depths of 20mm, 40 mm, 60 mm, 80 mm and 100 mm, in a descending order. The two vertical red lines bracket the duration of base disturbance. To the right of the second red line, the liquid is left to oscillate freely for the remainder of the 10-second period. The times for the occurrences of major peak energies are marked in Figures 2(a) and 2 (e) to help the relevant discussion.

In Figure 2, the shallow water levels in frames 2(a) and 2(b), seem to produce an irregular history with a steeper rate of decay of kinetic energy. As the water level gets deeper, particularly in frames 2(d) and 2(e), a more regular and periodic pattern seems to emerge. As the irregularities are lost to a periodic behaviour, the rate of energy dissipation becomes more gradual. The physical difference in between the two distinct behaviour patterns, is the existence of traveling waves for the shallow, and standing waves for the deep levels.

The shallowest water depth of 20 mm in Figure 2(a), has the most effective rate of energy dissipation. As in all other cases, the first second is the settling period allowed for the numerical algorithm. Excitation starts at 1 s from right to left. This excitation results in the formation of a traveling wave seen in Figure 3(a) at t = 1.27 s, at the right side of the container, traveling towards left. Snaphots of particular instances of simulation are presented in Figure 3. These snapshots indicate the velocities of all particles with the colour code whose scale is indicated below each frame.

Kinetic energy increases steadily after the generation of this first traveling wave. Then the container starts moving from left to right, causing a second traveling wave at the left side, traveling towards right. The instant of peak kinetic energy is shown in Figure 3(b) at t = 1.57 s, also showing the second traveling wave from the left side of the container.

The two opposing traveling waves collide immediately following the peak kinetic energy instant, at about $1/5^{th}$ the distance from the left side. In Figure 2(a), the sharp decrease in the total kinetic energy, following the peak energy, corresponds to the collision of the two waves. This sharp decrease in energy is due to the strong wave-to-wave interaction which causes a break of the sloshing surface as shown in Figure 3(c) at t = 1.73 s. At this point, it may be relevant to note that scale of velocities in Figure 3(c) is about one half of those in Figure 3(b).

Additionally in Figure 3(c), a small third wave is seen to be initiated at the right side of the container to lead to the following wave-to-wave interactions. In Figure 3(d), the snapshot at t = 1.81 s is presented that has partly descended surfaces following the interaction. This instant corresponds to the minor peak of kinetic energy in Figure 2(a).

Formation of the traveling waves, causes severe deflections of the free surface with complex velocity patterns. Invariably, the wave front has a discontinuous geometry which is the consequence of very steep velocity gradients. Hence, the wave front is the location of high shear stress and associated dissipation of kinetic energy.

In contrast to the 20mm-deep case in Figure 2(a), the 100 mm-deep case has the poorest rate of energy dissipation. History of kinetic energy for this case is given in Figure 2(e). Immediately following the right-to-left motion of the container, a wave starts to rise on the right side. The right wave travels towards left slowly, and merges with a severely rising wave on the left side, in response to the container changing direction towards right. The first dip observed in Figure 2(e) corresponds to the minimal kinetic energy at around 1.61 seconds, indicating peak displacement of the surface. Following this dip, kinetic energy rises steadily until 1. 82 seconds due to the contribution of the base excitation, and due to the settling of the surface to a nearly flat level.

As opposed to the discontinuous nature of the surface flow with shallow cases, the surface motion with 100 mm deep case assumes a periodic behaviour with smaller surface velocities. The second dip at t = 2.07 seconds, corresponds to the maximum surface deflection. This dip is followed by a peak corresponding to the settling to a flat surface, and maximum velocities. The following routine motion is consecutive rises on either walls of the container and descends. This routine wave motion is in the form of a standing wave, avoiding formation of traveling waves and wave-to-wave interactions.

Figures 3(e) and 3 (g) correspond to two of the wave-to-wall interactions at t= 2.07 s and t = 2.62 s where the kinetic energy plot makes a dip. Figures 3(f) and 3(h) are the snapshots

of t = 2.39 s and t = 2.85 s where the free surface is again close to being flat following consequent wave rises.

Kinetic energy plots of 40 mm, 60 mm and 80 mm deep cases are given in Figures 2(b) to 2(d). These cases represent the transition from the traveling waves, of the 20 mm deep case, to standing waves, of the 100 mm deep case. Not surprisingly, the 40 mm-deep case is similar to the shallowest case. The exception to this similarity, is the presence of the low amplitude oscillations that remain on the free surface without being dissipated. Various interacting traveling waves can be tracked for this case, by observing the presence of relatively sharp dips. The effect of the increasing depth is more noticeable for the 60 mm and 80 mm deep cases where regular oscillation patterns form with a slow rate of decay.

The fundamental sloshing frequency may be calculated using (Milne-Thomson, 1968)

$$f = \frac{1}{2\pi}\sqrt{\frac{g\pi}{d}\tanh(\frac{\pi h}{d})} \qquad (7)$$

where the frequency, f, is in Hz, for a container with length, d, filled to a depth of h. g is the acceleration due to gravity. For the 80 mm and 100 mm deep cases, the theoretical values of the fundamental sloshing frequency are calculated to be 1.0 Hz and 1.1 Hz, respectively. These frequencies correspond to those of numerical predictions in this study.

In Figures 4(a) and 4(b), probability distributions of the kinetic energy are given for the shallowest and the deepest cases. As expected, the travelling waves severely limit the available energy to the smallest levels in Figure 4(a). Almost half the total simulation is represented within the first bar for the shallowest case. In Figure 4(b), there is a more gradual distribution of the mid-level kinetic energy instances, indicating the large fraction of time allocated to these levels of energy. Only $1/5^{th}$ of the simulation is represented in the first bar.

In Figure 5, 70%, 80% and 90% settling times of all five cases are given. A settling time is defined as the required duration for the total kinetic energy to decay below a certain fraction of its maximum value. For instance, 70% settling time indicates how long a duration is required to dissipate 70% of the peak kinetic energy. As expected, shallow levels settle at shorter times. The two deeper levels of 80 mm and 100 mm, do not reach their 90% settling time within the total simulation period of 10 seconds.

The percentage remainder energy in the system after 10 seconds is given in Figure 6. Almost no remainder energy is observed for the shallowest case, whereas the level of the remainder energy increase monotonically until the 100 mm deep case. Nearly $1/5^{th}$ of the peak energy remains for the 100 mm deep case at the end of 10 seconds.

CONCLUSIONS

Dissipation of kinetic energy due to shearing of the liquid, is observed to be the primary means of energy loss. Traveling waves are able to provide steep gradients of velocity to improve energy dissipation. In addition, a traveling wave can interact with another to dissipate energy effectively. Traveling waves are only generated in shallow levels of liquid. As the liquid level gets deeper, sloshing tends to be more of standing wave type with poorer dissipation characteristics.

Numerical observations indicate that the shallowest level of liquid to be the most effective energy dissipator. It should be understood that no effort is reported here on the significance of tuning the container dimensions to affect dissipation.

Finally, observations from a series of numerical case studies are presented in this paper. They only represent predictions, and need to be verified with experiments.

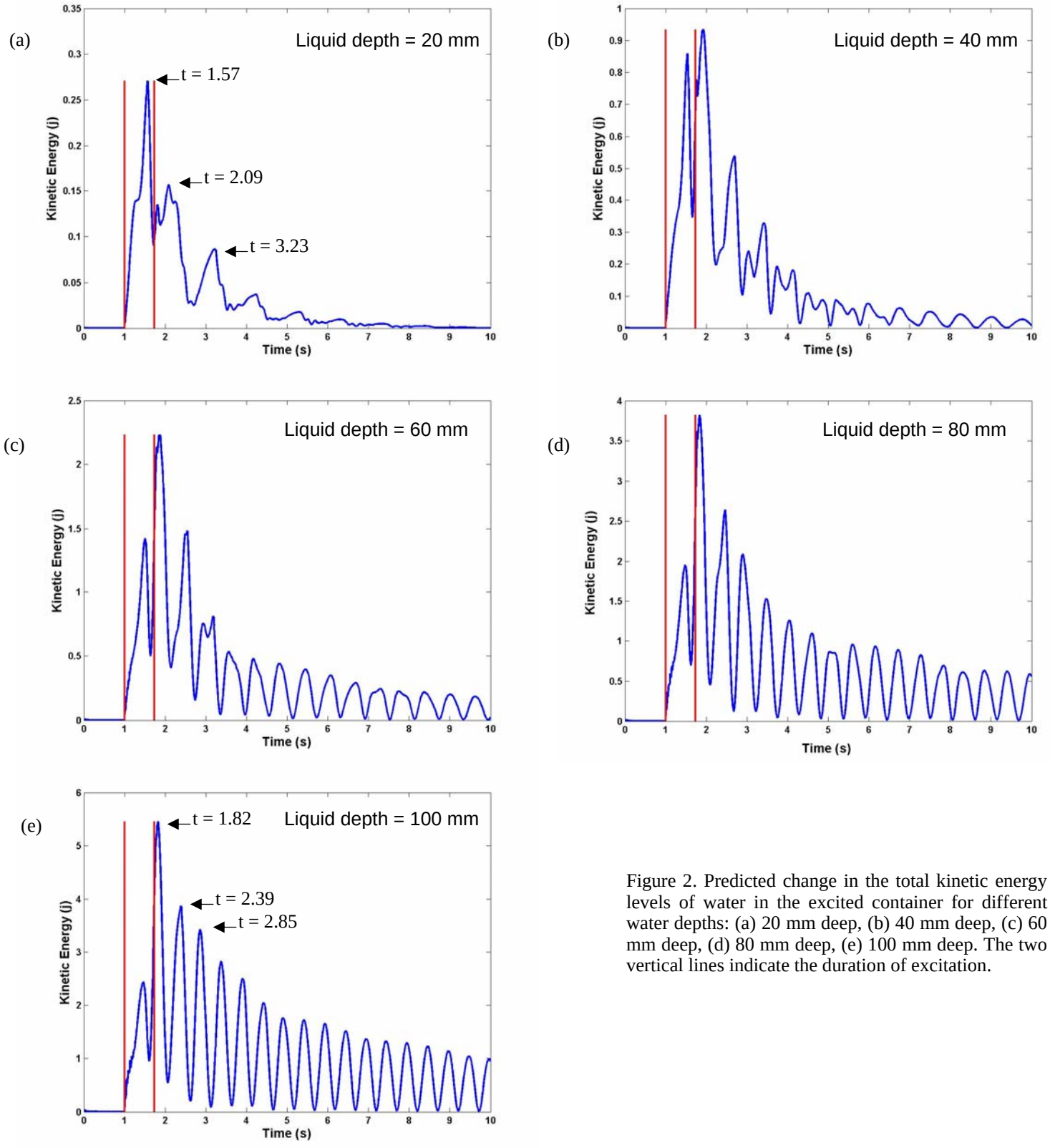

Figure 2. Predicted change in the total kinetic energy levels of water in the excited container for different water depths: (a) 20 mm deep, (b) 40 mm deep, (c) 60 mm deep, (d) 80 mm deep, (e) 100 mm deep. The two vertical lines indicate the duration of excitation.

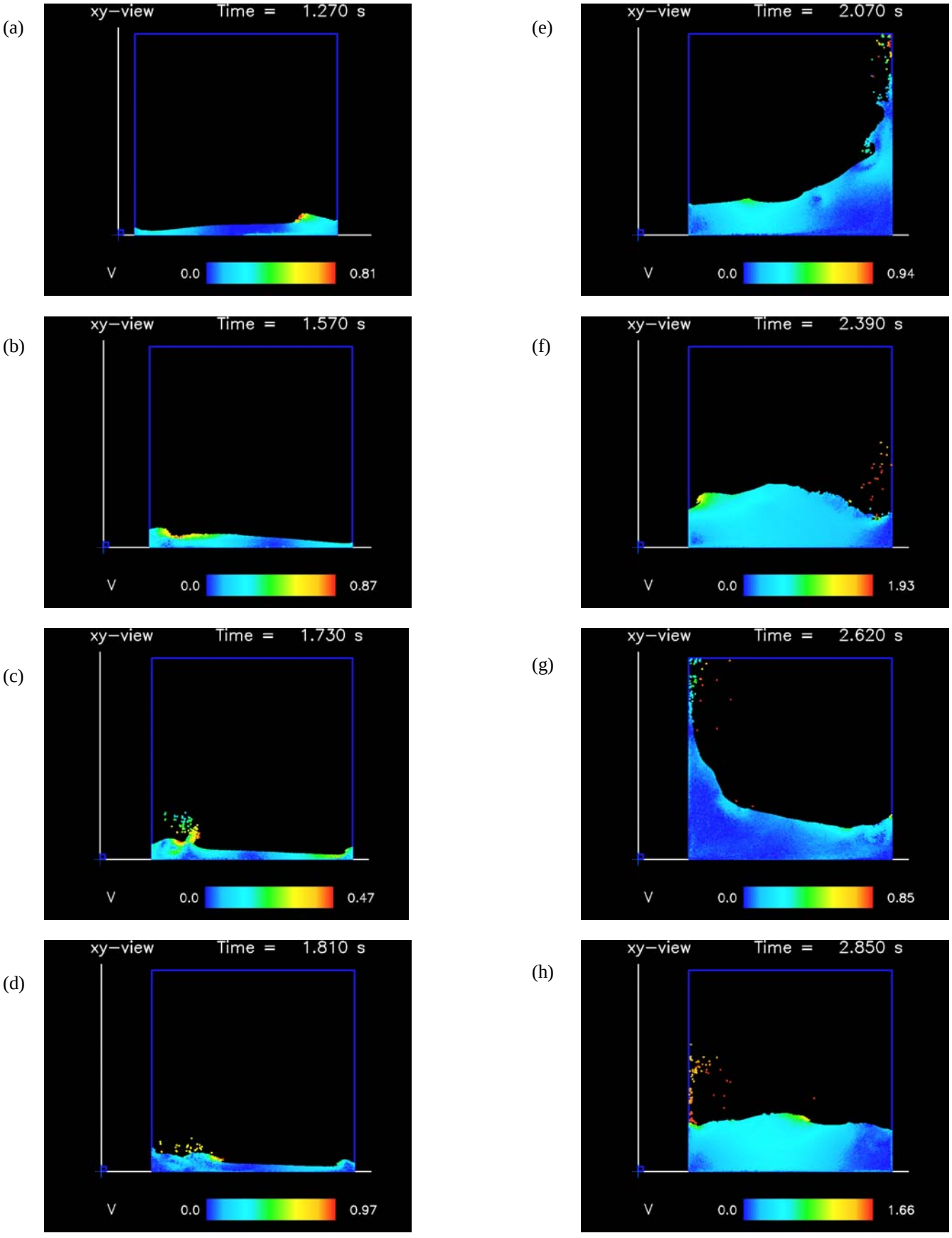

Figure 3. Snapshots of various instants of interest. First column corresponds to 20 mm deep water, second column corresponds to 100 mm deep water

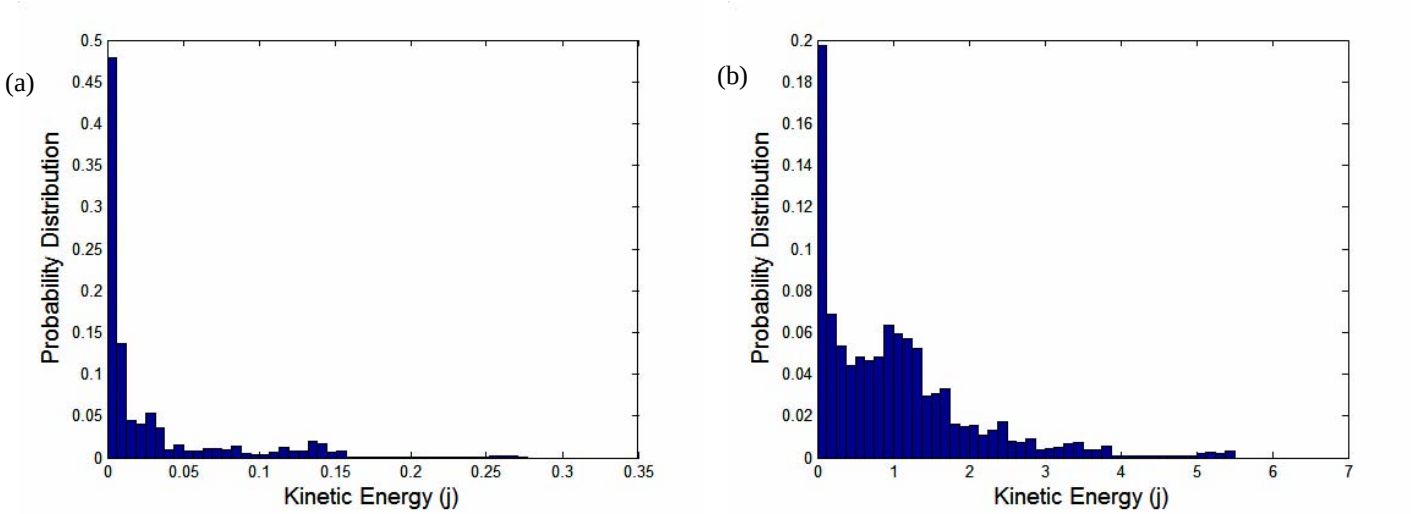

Figure 4. Distribution of kinetic energy values for the shallowest and deepest cases: (a) 20 mm deep, (b) 100 mm deep.

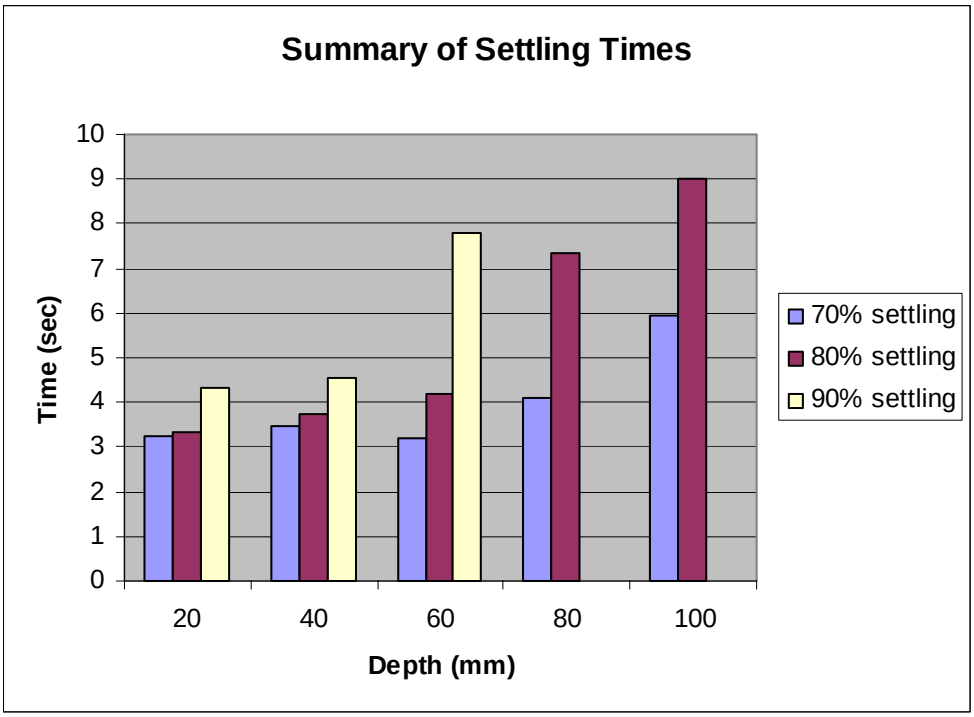

Figure 5. A summary histogram of settling times for different water depths.

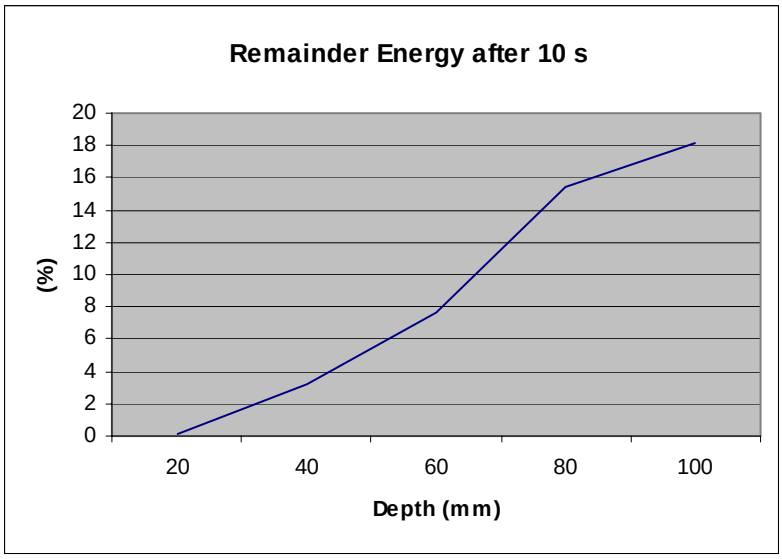

Figure 6. Percentage remainder energy after 10 seconds, for varying water depths.

REFERENCES

[1] Modi, V. J., and Seto, V. L., 1997, "Suppression of Flow Induced Oscillations Using Sloshing Liquid Dampers: Analysis and Experiments", J. of Wind Eng. & Ind. Aerodyn., **67&68**, pp. 611-625.

[2] Reed, D., Yeh, H., Yu, J., and Gardarsson, S., 1998, "Tuned Liquid Dampers under Large Amplitude Excitation", J. of Wind Eng. & Ind. Aerodyn., **74-76**, pp. 923-930.

[3] Banerji, P., Murudi, M., Shah, A., H., and Popplewell, N., 2000, "Tuned Liquid Dampers for Controlling Earthquake Response of Structures", Eartquake Engng. Struct. Dyn., **29**, pp. 587-602.

[4] Shankar, K., and Balendra, T., 2002, "Application of the Energy Flow Method to Vibration Control of Buildings with Multiple Tuned Liquid Dampers", J. of Wind Eng. & Ind. Aerodyn., **90**, pp. 1893-1906.

[5] Li, S., J., Li, G., Q., Tang, J., and Li, Q., S., 2002, "Shallow Rectangular TLD for Structural Control Implementation", Applied Acoustics, **63**, pp. 1125-1135.

[6] Cleary, P. W., and Prakash, M., 2004, "Discrete-Element Modelling and Smoothed Particle Hydrodynamics: Potential in the Environmental Sciences", Phil. Trans. R. Soc. Lond., **362**, pp. 2003-2030.

[7] Iglesias, A., S., Rojas, L., P., and Rodriguez, R., Z., 2004, "Simulation of Anti-Roll Tanks and Sloshing Type Problems with Smoothed Particle Hydrodynamics", Ocean Engng., **31**, pp. 1169-1192.

[8] Monaghan, J. J., 1994, "Simulating free surface flows with SPH", J. Comp. Phys., **110**, pp. 399-406.